



Selective tuning of activity in a multifunctional enzyme as revealed in the F21W mutant of dehaloperoxidase B from *Amphitrite ornata*

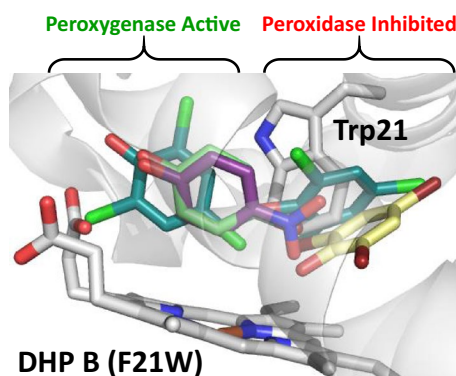
Leiah M. Carey¹ · Kyung Beom Kim^{1,2} · Nikolette L. McCombs¹ · Paul Swartz³ · Cheal Kim² · Reza A. Ghiladi¹

Received: 28 September 2017 / Accepted: 17 November 2017
© SBIC 2017

Abstract

Possessing both peroxidase and peroxygenase activities with a broad substrate profile that includes phenols, indoles, and pyrroles, the enzyme dehaloperoxidase (DHP) from *Amphitrite ornata* is a multifunctional catalytic hemoglobin that challenges many of the assumptions behind the well-established structure–function paradigm in hemoproteins. While previous studies have demonstrated that the F21W variant leads to attenuated peroxidase activity in DHP, here we have studied the impact of this mutation on peroxygenase activity to determine if it is possible to selectively tune DHP to favor one function over another. Biochemical assays with DHP B (F21W) revealed minimal decreases in peroxygenase activity of 1.2–2.1-fold as measured by 4-nitrophenol or 5-Br-indole substrate conversion, whereas the peroxidase activity catalytic efficiency for 2,4,6-trichlorophenol (TCP) was more than sevenfold decreased. Binding studies showed a 20-fold weaker affinity for 5-bromoindole ($K_d = 2960 \pm 940 \mu\text{M}$) in DHP B (F21W) compared to WT DHP B. Stopped-flow UV/visible studies and isotope labeling experiments together suggest that the F21W mutation neither significantly changes the nature of the catalytic intermediates, nor alters the mechanisms that have been established for peroxidase and peroxygenase activities in DHP. The X-ray crystal structure (1.96 Å; PDB 5VLX) of DHP B (F21W) revealed that the tryptophan blocks one of the two identified TCP binding sites, specifically TCP_{interior}, suggesting that the other site, TCP_{exterior}, remains viable for binding peroxygenase substrates. Taken together, these studies demonstrate that blocking the TCP_{interior} binding site in DHP selectively favors peroxygenase activity at the expense of its peroxidase activity.

Graphical abstract



Keywords Globin · Peroxidase · Peroxygenase · Structure–function relationship

Electronic supplementary material The online version of this article (<https://doi.org/10.1007/s00775-017-1520-x>) contains supplementary material, which is available to authorized users.

Extended author information available on the last page of the article

Introduction

The coelomic hemoglobin of the sediment-dwelling marine worm *Amphitrite ornata* functions as a naturally occurring dehalogenation enzyme that has been termed

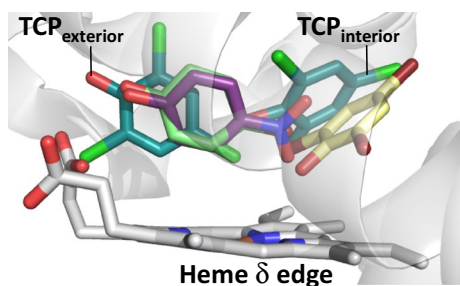


Fig. 1 Superposition of substrate binding sites within the distal pocket of DHP as viewed from the heme γ edge: TBP (yellow, PDB 4FH7 [27]), 4-NP (purple, PDB 5CHQ [4]), 4-BP (green, PDB 3LB2 [26]), and both internal (TCP_{interior}) and external (TCP_{exterior}) conformations of TCP (cyan, PDB 4KN3 [24])

dehaloperoxidase (DHP) [1, 2]. In addition to being able to oxidize/degrade 7 EPA priority pollutants of phenolic structure (phenol, 2-chlorophenol, 2,4-dichlorophenol, 2,4,6-trichlorophenol, 2-nitrophenol, 4-nitrophenol, and 2,4-dinitrophenol) [3, 4], DHP more broadly has shown activity against halogenated indoles [5], pyrroles [6], and guaiacols. Mechanistic studies [7–18] have shown that DHP appears to function via a Poulos–Kraut type mechanism [19] in which H_2O_2 reacts with a ferric heme to form DHP compound I [13, 16], the iron(IV)-oxo (ferryl) porphyrin π -cation radical species that is common to both the peroxidase [20] and P450 cycles [21]. Accordingly, DHP acts on the aforementioned substrates with peroxidase [2, 22], peroxygenase [5, 6], and oxidase [5] mechanisms. Moreover, DHP is known to bind a number of persistent organic pollutants (POPs) belonging to the azole class of compounds [23], including benzotriazole, benzimidazole, indazole, and imidazole that have widespread agricultural and industrial uses. Thus, given the broad substrate scope and multiple catalytic activities exhibited by DHP, one of the outstanding questions is how substrate binding is related to enzyme activity in this multifunctional and promiscuous catalytic globin, and whether DHP can be tuned to favor one activity over another.

One of the key features of DHP that sets it apart from traditionally studied globins (e.g., myoglobin and hemoglobin), and even many heme peroxidases, is that it possesses a distal small molecule binding site that can accommodate a variety of different substrates (and inhibitors) [1, 2, 24, 25], examples of which are shown in Fig. 1 and include the peroxygenase substrate 4-nitrophenol (4-NP, purple, PDB 5CHQ [4]), inhibitor 4-bromophenol (4-BP, PDB 3LB2 [26]), and the peroxidase substrates 2,4,6-tribromophenol (TBP, yellow, PDB 4FH7 [27]) and 2,4,6-trichlorophenol (TCP, cyan, PDB 4KN3 [24]). Two substrate binding sites were determined for TCP [TCP_{interior} (near the heme α edge) and TCP_{exterior} (near the heme γ edge and heme cavity)], while TBP was

observed to bind in a single site and in a similar orientation as TCP_{interior}. The observation of multiple binding sites across the entire face of the distal heme cavity is consistent with DHP being a multifunctional catalytic globin. More importantly, one can evaluate the orientation of binding for these substrates in Fig. 1 against the activities that each is subjected to: the unhindered (at the C2 and C3 positions) nitrophenol substrate is susceptible to DHP peroxygenase activity, possibly via an electrophilic addition by the ferryl intermediate, leading to incorporation of the O atom from hydrogen peroxide [4]. By contrast, the comparable positions in TBP are sterically hindered by the halogen substituents, precluding O atom transfer, and leading to substrate oxidation via a peroxidase mechanism [27]. TCP binds as a peroxidase substrate (i.e., TCP_{interior}) in a conformation that closely resembles that observed for TBP, but self-inhibition at high concentrations has also been observed [24], and has been attributed to the TCP_{exterior} site as this conformation orients the para-halogen above the heme iron and to the detriment of H_2O_2 -binding. Although currently there is no indole-bound structure of DHP, both computational studies of haloindole binding [5] and X-ray structures with bound azoles [23] (as models for indole) strongly suggest that indoles bind in an orientation relative to the ferryl heme that facilitates O atom transfer via a peroxygenase mechanism.

Following the identification of the two TCP binding sites in DHP, Dawson and co-workers rationally designed the F21W mutation in DHP A to block one of those sites, TCP_{interior} [24]. Modeling revealed that the potential W21 rotamers of the mutant either blocked the TCP_{interior} site, or were disallowed because of steric hindrance with the protein. The consequence of the F21W mutation was a 15-fold reduction in catalytic efficiency ($k_{\text{cat}}/K_{\text{M}}^{\text{TCP}}$) vs WT DHP A for peroxidase activity with TCP as the substrate, thus confirming their hypothesis that mutagenesis of F21 to the larger Trp residue would significantly impair peroxidase activity. At that time, however, the peroxygenase [4–6] activity of DHP was not known, and the consequence of the F21W mutation on that activity was unexplored. Given the recent identification of the 4-nitrophenol peroxygenase substrate binding site [4] that does not overlap significantly with TCP_{interior}, and the unknown consequence of the F21W mutation on peroxygenase activity, we were motivated to explore this mutation as a possible means of selectively tuning the activity profile of DHP. To that end, we present here a study of the DHP B (F21W) mutant on peroxygenase activity, including biochemical assays, stopped-flow UV–visible spectroscopic characterization of the activated enzyme, as well as an X-ray crystallographic study of the mutant. The results demonstrate the ability to favor peroxygenase activity over peroxidase activity in a rationally designed mutant of a multifunctional catalytic globin.

Experimental

Materials

Unless otherwise specified, all chemicals were of reagent grade, purchased from VWR or Fisher Scientific, and used without further purification. $\text{H}_2^{18}\text{O}_2$ and H_2^{18}O (90 and 98% oxygen atom enriched, respectively) were obtained from ICON Isotopes (Summit, NJ, USA). DHP was expressed, purified and obtained in the ferric oxidation state as previously reported [9]. The enzyme concentration was determined spectrophotometrically using the molar absorptivity coefficient ($\epsilon_{406} = 116,400 \text{ M}^{-1} \text{ cm}^{-1}$ [9]). Stock solutions (2 mM) of trichlorophenol (TCP) were prepared in 100 mM potassium phosphate (KP_i) buffer (pH 7) and stored at -80°C . TCP concentration and lack of degradation was monitored by measuring its absorbance at 312 nm ($\epsilon = 3752 \text{ M}^{-1} \text{ cm}^{-1}$ [8]). Stock solutions (10 mM) of 5-bromoindole and 7-bromoindole were prepared in MeOH, stored at -80°C in glass vials, and screened by HPLC for degradation prior to use [5]. Aliquots were stored on ice during use. Stock solutions (5 mM) of 4-nitrophenol (4-NP) were prepared fresh in 100 mM KPi (pH 7) when needed. Solutions of H_2O_2 were prepared daily, and stored on ice while protected from light until needed. The concentration of H_2O_2 was determined spectrophotometrically ($\epsilon_{240} = 43.6 \text{ M}^{-1} \text{ cm}^{-1}$ [28]).

Construction of mutant DHP plasmid

Site-directed mutagenesis was performed using the Quikchange II site-directed mutagenesis kit (Agilent Technologies). Mutagenesis [melt (95°C , 60 s), anneal (55°C , 50 s), and extension (68°C , 360 s)] was performed for 16 cycles. Oligonucleotides were synthesized by Integrated DNA Technologies (IDT) (sense 5'-ACC TAT GCA CAG GAC ATT TGG CTC GCA TTT TTG AAT AGG-3'; anti-sense 5'-CCT ATT CAA AAA TGC GAG CCA AAT GTC CTG TGC ATA GGT-3'). The plasmid encoding a N-terminal poly-His tag wild-type DHP B was used as a template [9]. For crystallization, the mutant was obtained from a plasmid-encoding wild-type DHP B lacking the N-terminal poly-His tag [18]. The modified plasmids were transformed into *E. coli* BL21-Gold(DE3) competent cells (Agilent Technologies) and selected based on survival on LB-agar-ampicillin (100 $\mu\text{g}/\text{mL}$) plates. The plasmids were extracted using the spin column plasmid DNA kit (Bio Basic), and the desired mutation and lack of deleterious secondary ones were confirmed by sequencing (Genewiz).

Protein crystallization and X-ray diffraction studies

Non-His tagged DHP B (F21W) was overexpressed and purified following the literature protocol [4]. Crystals were obtained through the hanging-drop vapor diffusion method. DHPB (F21W), in 20 mM Na cacodylate buffer pH 6.4, was concentrated to 12 mg/mL, and the crystals were grown from mother liquor solutions of 28–32% PEG 4000 and 0.2 M ammonium sulfate at pH 6.4, equilibrated against identical reservoir solutions. Protein-to-mother liquor ratios varied between 1:1, 1.33:1, 1.66:1 and 2:1. At 4°C , crystals grew from each condition after 3 days. The crystals were cryo-protected by briefly dipping them in reservoir solution enhanced with 20% glycerol and then flash frozen in liquid N_2 . Data were collected at the Biological X-ray Facility at NCSU on a Rigaku RuH3R with rotating copper anode equipped with a MAR345 CCD image plate detector and Oxford cryojet set at 100 K, utilizing a wavelength of 1.54 Å. All data were scaled and integrated using HKL2000 [29], molecular replacement was performed with Phaser-MR [30] from the PHENIX [31] suite of programs using the 3IXF [18] monomer as the search model, model building and manual placement of waters utilized COOT [32] and refinement was carried out using phenix.refine [33].

Peroxidase studies

The hydrogen peroxide-dependent oxidative dehalogenation of 2,4,6-trichlorophenol (TCP) to 2,6-dichloro-1,4-benzoquinone (DCQ) as catalyzed by DHP was measured using a Cary 50 UV-Vis spectrophotometer. The reactions were performed in triplicate at pH 7 in 100 mM KPi at 25°C , with a 1 mL total reaction volume. Buffered solutions of DHP (1.25 μM) and TCP (10–800 μM) were premixed and the reaction was initiated by the addition of H_2O_2 (80 μM). The change in absorbance at 272 nm (DCQ, $\epsilon = 14 \text{ mM}^{-1} \text{ cm}^{-1}$ [7]) was measured using Cary WinUV Kinetics software over a 30 s time frame with a rate of 1 scan per second. The data were fit to the standard Michaelis–Menten kinetics model using the method of initial rates in the Grafit software package (Erithacus Software). The apparent kinetics parameters K_M and k_{cat} resulted from the optimization of the fitting procedure.

Peroxygenase studies

The percent conversions of 5-Br-indole, 7-Br-indole and 4-nitrophenol (4-NP) as catalyzed by DHP in the presence of H_2O_2 were analyzed by HPLC using a Waters 2796 Bioseparations Module coupled with a Waters 2996 Photodiode Array Detector and equipped with an ODS Hypersil C_{18} column (Thermo-Scientific, 150 mm \times 4.6 mm, 5 μm particle size). The reactions were performed in triplicate in

100 mM KP_i (pH 7) at 25 °C. Indole reactions also contained 5% MeOH (v/v). Buffered solutions of substrate and DHP were premixed, and the peroxxygenase reaction was initiated with addition of H_2O_2 . Final concentrations were 10 μM DHP, 500 μM substrate and 500 μM H_2O_2 in 200 μL total volume. After 5 min of incubation at 25 °C, the reaction was quenched with excess catalase and then diluted 1:10 with 1800 μL of 100 mM KP_i (pH 7). Diluted samples were subjected to HPLC analysis (solvent A— H_2O containing 0.1% trifluoroacetic acid; solvent B—HPLC-grade MeCN containing 0.1% trifluoroacetic acid). The elution method was as follows: 1.5 mL/min of 95:5 (A:B) to 5:95 using a linear gradient over 10 min; 5:95 isocratic for 2 min; 5:95–95:5 using a linear gradient over 1 min, and then isocratic for 4 min. Analysis was performed using the Empower software package (Waters Corp.).

5-Br-indole binding studies

As adapted from previously published protocols [5, 34], the 5-Br-indole dissociation constant (K_d) was determined in triplicate for DHP in 100 mM KP_i (pH 7) containing 10% MeOH at 25 °C using a Cary 50 UV–Vis spectrophotometer. A stock solution of 10 mM 5-Br-indole in MeOH was prepared in a glass vial. The UV–Vis spectrophotometer was referenced with 10 μM ferric DHP in 100 mM KP_i (pH 7) containing 10% MeOH (v/v). The total volume of the samples was 200 μL with final concentrations of 10 μM ferric DHP and 10–130 equivalents 5-Br-indole while maintaining 10% MeOH (v/v). Perturbations in the absorbance of the Soret band (ΔAbs) were recorded for each 5-Br-indole concentration (Figure S1). Analysis by nonlinear regression using the GraFit software package (Erithacus Software Ltd.) provided a calculated A_{max} , which was used to calculate α ($\Delta A/\Delta A_{\text{max}}$) for the average ΔA for each concentration. A nonlinear regression plot provided the reported K_d values.

Stopped-flow UV–visible studies

Optical spectra were recorded using a Bio-Logic SFM-400 triple-mixing stopped-flow instrument coupled to a rapid scanning diode array UV–visible spectrophotometer. The reactions were conducted at room temperature, and all solutions were prepared in 100 mM KP_i (pH 7). Data were collected (900 scans total) over a three-time domain regime (2.5, 25, and 250 ms; 300 scans each) using the Bio Kinet32 software package (Bio-Logic). All data were evaluated using the Specfit Global Analysis System software package (Spectrum Software Associates) and fit to exponential functions as two-step/three-species irreversible mechanisms. Experiments were performed in single-mixing mode where DHP B (F21W) at a final concentration of 10 μM was reacted with 2.5–25 equivalents of H_2O_2 .

Results

Overexpression, purification and characterization of DHP B

Recombinant DHP B (F21W) was obtained by expression in *E. coli* and purified as previously described [4, 9, 18]. The monomeric molecular weight of DHP B (F21W) was determined by electrospray ionization MS to be 16,313.11 g/mol, in good agreement with the theoretical expected value (16,313.42 g/mol). DHP B (F21W) was initially isolated as a mixture of the ferric and oxyferrous forms, as were WT isoenzymes A and B [8, 9], and subsequent treatment with an excess of potassium ferricyanide permitted the isolation of the ferric form. The electronic absorption spectrum of ferric DHP B (F21W) exhibited features typical of a high-spin ferric heme [UV–visible: 407 (Soret), 504, 634 nm; Fig. 2] that were similar to those observed previously for WT DHP B [UV–visible: 407 (Soret), 508, 633 nm] [9]. The optical purity ratio (Reinheitzahl or R_z , defined as A_{Soret}/A_{280}) for DHP B (F21W), was found to be 3.63, lower than the literature value for WT DHP B of 4.1 [9, 13]. This was expected, however, as the F21W mutation increases the calculated A_{280} molar absorptivity coefficient to 16,960 $\text{M}^{-1} \text{cm}^{-1}$ in DHP B (F21W) from 11,460 $\text{M}^{-1} \text{cm}^{-1}$ in WT DHP B. The A_{Soret}/A_{380} (1.87) ratio for DHP B (F21W) was also similar to that for WT DHP B ($A_{\text{Soret}}/A_{380} = 1.88$; $A_{614}/A_{645} = 1.14$) [9, 13]. However, the A_{614}/A_{645} (0.93) ratio was lower in the F21W mutant, suggesting a slightly lower population of six-coordinate high-spin heme in the mutant when compared to its wild-type analog. Sodium dithionite reduction of the ferric enzyme in the presence of O_2 yielded oxyferrous DHP B (F21W), with spectral features [UV–visible: 418 (Soret), 544, 578 nm] that were again

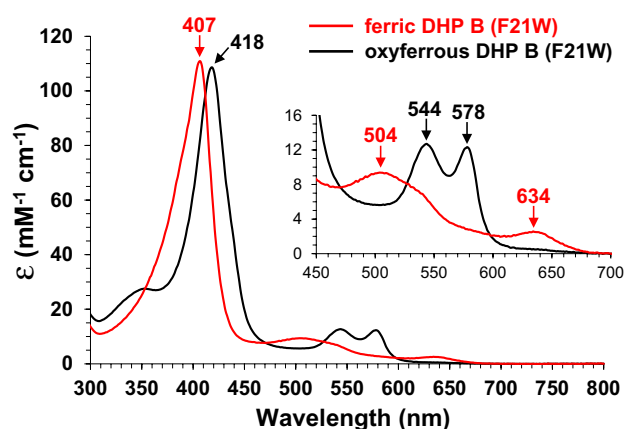


Fig. 2 UV–visible spectra of ferric (red) and oxyferrous (black) DHP B (F21W) in 100 mM KP_i (pH 7)

consistent with the six-coordinate low-spin oxyferrous forms of the wild-type isoenzymes [8, 9].

Activity assays

The peroxidase activity of DHP for the oxidative dehalogenation of 2,4,6-trichlorophenol (TCP) to 2,6-dichloro-1,4-benzoquinone (DCQ) was monitored spectrophotometrically in a (TCP)-dependent manner at a fixed concentration of H_2O_2 . When compared with the kinetic parameters of WT DHP B (Table 1; $k_{\text{cat}} = 1.90 \pm 0.20 \text{ s}^{-1}$; $K_{\text{M}} = 90 \pm 20 \mu\text{M}$; $k_{\text{cat}}/K_{\text{M}} = 21 \pm 5 \text{ mM}^{-1} \text{ s}^{-1}$), DHP B (F21W) exhibited a 1.5-fold decrease in catalytic turnover ($k_{\text{cat}} = 1.29 \pm 0.07 \text{ s}^{-1}$), a 4.9-fold increase in K_{M} ($440 \pm 50 \mu\text{M}$), and a 7.2-fold lower catalytic efficiency ($k_{\text{cat}}/K_{\text{M}} = 2.9 \pm 0.3 \text{ mM}^{-1} \text{ s}^{-1}$). These results demonstrate that the F21W mutation significantly affects the peroxidase activity of DHP B, but the effect is less pronounced than observed for DHP A (F21W) when compared to WT DHP A (3.3-fold lower k_{cat} , 4.6-fold higher K_{M} , and 15-fold lower $k_{\text{cat}}/K_{\text{M}}$) [24]. When 4-bromophenol ($K_{\text{d}} = 1.15 \text{ mM}$ [26]), the known inhibitor of DHP peroxidase and peroxygenase activities [5, 9], was included in the reaction at $500 \mu\text{M}$, the rate of TCP oxidation as catalyzed by the F21W mutant was reduced by 45%.

The peroxygenase activity of DHP was monitored by HPLC for the H_2O_2 -dependent oxidation of 5-Br-indole, 7-Br-indole, and 4-nitrophenol (4-NP) when initiated from the ferric state at pH 7. Overall, the effect of the F21W mutation on substrate percent conversion was limited: the DHP B (F21W) mutant exhibited a decrease of: (i) 1.4-fold for 5-Br-indole (34.0 ± 1.6 vs $48.1 \pm 2.3\%$ for WT DHP B [5]), (ii) 1.2-fold for 7-Br-indole (39.4 ± 1.2 vs $46.1 \pm 1.7\%$ for WT DHP B [5]), and (iii) 2.1-fold for 4-NP (19.1 ± 0.3 vs $39.4 \pm 0.7\%$ for WT DHP B [4]). As peroxygenase activity was not known at the time when Dawson and co-workers [24] first described the effects of the F21W mutation on the catalytic (peroxidase) activity of DHP, no data for DHP A (F21W) are available. However, when compared with WT DHP A, the reactivity of DHP B (F21W) with 5-Br-indole is

higher by 1.7-fold (34.0 ± 1.6 vs $20.3 \pm 1.7\%$ for WT DHP A [5]), while the 4-NP reactivity is approximately equivalent (19.1 ± 0.3 vs $21.6 \pm 0.1\%$ for WT DHP A [4]). As was the case for peroxidase activity, inclusion of $500 \mu\text{M}$ 4-bromophenol as an inhibitor attenuated 5-Br-indole substrate conversion to $4.6 \pm 1.4\%$.

Isotopically labeled oxygen studies

Studies employing labeled $\text{H}_2^{18}\text{O}_2$ and H_2^{18}O (90 and 98% oxygen atom enriched, respectively) were performed with 5-Br-indole and subsequently analyzed by LC-MS to confirm hydrogen peroxide as the source of the O atom incorporated in the peroxygenase studies. The background-subtracted total ion chromatograms (TICs) are shown in Fig. 3 for the 5-Br-2-oxindole product. Reactions performed in the presence of H_2^{18}O and unlabeled H_2O_2 show 5-Br-2-oxindole (m/z 212, 214; Fig. 3a) with product m/z values identical to those obtained from the unlabeled $\text{H}_2\text{O}/\text{H}_2\text{O}_2$ reaction. Gratifyingly, the reactions performed in the presence of $\text{H}_2^{18}\text{O}_2$ in unlabeled H_2O exhibited the characteristic m/z shift of +2 amu (Fig. 3b), denoting ^{18}O -label incorporation. Similarly, the 5-Br-3-oxindolenine (m/z 210, 212) product only showed a shift of +2 amu in the presence of labeled $\text{H}_2^{18}\text{O}_2$ (data not shown). Taken together, the labeling studies confirmed that the oxygen atom incorporated into the products was derived solely from H_2O_2 , thus demonstrating that the F21W mutation does not alter the reported peroxygenase chemistry.

Stopped-flow UV-visible spectroscopy

To assess the ability of DHP B (F21W) to form compound ES, the catalytically active two-electron-oxidized state containing both a ferryl center [$\text{Fe}^{\text{IV}}=\text{O}$] and a tyrosyl radical, single-mixing stopped-flow UV-visible spectroscopic methods were employed as previously described [8, 9]. Using the 10-eq. H_2O_2 reaction as representative data (Fig. 4), the following observations were made: an SVD analysis employing a simple three component, irreversible

Table 1 Kinetic parameters for the oxidation of TCP, and percent substrate conversion for the oxygenation of 5-Br-indole, 7-Br-indole and 4-NP

Enzyme	Peroxidase ^a			Peroxygenase ^{a,b}			Refs.
	$K_{\text{M}}^{\text{TCP}}$ (μM)	k_{cat} (s^{-1})	$k_{\text{cat}}/K_{\text{M}}$ ($\text{mM}^{-1} \text{ s}^{-1}$)	5-Br-indole	7-Br-indole	4-nitrophenol	
DHP B (F21W)	440 ± 50	1.29 ± 0.07	2.9 ± 0.3	34.0 ± 1.6	39.4 ± 1.0	19.1 ± 0.3	^c
WT DHP B	90 ± 20	1.90 ± 0.20	21 ± 5	48.1 ± 2.3	46.1 ± 1.7	39.4 ± 0.7	^c
DHP A (F21W)	2260 ± 512	0.32 ± 0.05	0.14 ± 0.03	n/a	n/a	n/a	[24]
WT DHP A	495 ± 62	1.05 ± 0.07	2.1 ± 0.3	20.3 ± 1.7	n/a	21.6 ± 0.1	[4, 5, 24]

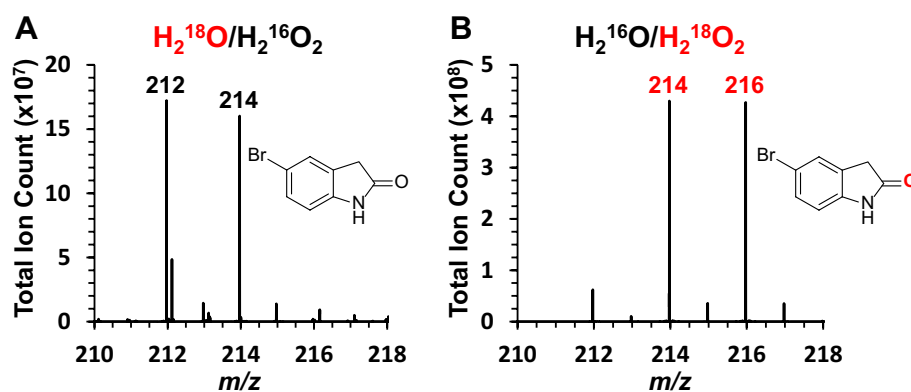
n/a not available

^a Reactions were performed with ferric DHP in 100 mM KP_i buffer (pH 7) at 25°C

^b Values represent percent (%) substrate conversion

^c This work

Fig. 3 ESI-MS total ion chromatograms obtained for the reaction product 5-Br-2-oxindole (A: H_2^{18}O , $\text{H}_2^{16}\text{O}_2$; B: H_2^{16}O , $\text{H}_2^{18}\text{O}_2$). Reaction conditions: $[\text{5-Br-indole}] = [\text{H}_2\text{O}_2] = 500 \mu\text{M}$, $[\text{enzyme}] = 10 \mu\text{M}$, 100 mM KP_i (pH 7), 25°C



mechanism (a→b→c) revealed that upon rapid mixing (2 ms) of a ferric DHP B (F21W) solution [UV–visible spectrum: 407 (Soret), 505, 535 (sh), 635] with 10 equiv H_2O_2 , a new species was observed whose spectral features [UV–visible: 419 (Soret), 545, 587 nm] we attributed to the ferryl-containing intermediate compound ES based upon our previous assignments of this reaction intermediate in WT DHP A [8] and B [9]. The experimental value of k_{obs} for compound ES formation varied linearly with hydrogen peroxide concentration (2.5–25 mol equiv), from which the bimolecular rate constant was determined to be $(6.68 \pm 0.05) \times 10^4 \text{ M}^{-1} \text{ s}^{-1}$, in agreement with the values reported for WT isoenzymes [DHP A: $(3.56 \pm 0.02) \times 10^4 \text{ M}^{-1} \text{ s}^{-1}$ [8]; DHP B: $(1.29 \pm 0.11) \times 10^5 \text{ M}^{-1} \text{ s}^{-1}$ [9]; Table 2]. The DHP B (F21W) compound ES intermediate further converted to a new species [UV–visible: 412 (Soret), 535, 565 (sh) nm; $k_{\text{obs}} = 0.012 \pm 0.001 \text{ s}^{-1}$]. We have assigned this as compound RH, the “reversible heme” state of dehaloperoxidase that forms from the decay of compound ES in the absence of a co-substrate, for this variant based upon analogy to the similar, but not identical, species observed in DHP isoenzymes A [411 (Soret), 530, 564 (sh) nm; $k_{\text{obs}} = 0.0167 \pm 0.0003 \text{ s}^{-1}$] [8] and B [411 (Soret), 554, 599 (sh) nm; $k_{\text{obs}} = 0.010 \pm 0.001 \text{ s}^{-1}$] [9], as well as in various other DHP mutants [13].

X-ray crystallographic studies

Non-His tagged DHP B (F21W) was overexpressed, purified, crystallized, and its structure solved by X-ray diffraction methods. X-ray data collection and refinement statistics are provided in Table 3. DHP B (F21W) refined to a resolution of 1.96 \AA , with R_{merge} , R_{work} and R_{free} values of 8.4, 16.43 and 20.45%, respectively.

DHP B (F21W) crystallized as a homo-dimer in the asymmetric unit of the $\text{P}2_12_12_1$ space group, consistent with all previous DHP crystal structures. The protomer environments were identical, as shown through the global least squared quadratic (LSQ) C^α superpositions: the root

mean squared deviation (rmsd) value of 0.3194 \AA for the DHP B (F21W) superposition of protomers A and B is consistent with highly homologous structures that possess very little geometric variation over conformational space [35–37]. LSQ C^α superposition of DHP B (F21W) and WT DHP B yielded a rmsd value of 0.3491 \AA (average of subunits), which again shows high structural similarity globally. Moreover, the hemes align very well despite not being a variable in the C^α LSQ alignment (Fig. 5a).

As opposed to the global comparison, a closer inspection of the F21W mutant active site (Fig. 5b) revealed differences from previous DHP structures (Fig. S2): the ferric DHP B (F21W) structure shows the absence of the usual water molecule as the heme-Fe sixth ligand. Rather, unique to this DHP structure is the presence of two water molecules in the distal pocket that form a hydrogen-bonding network with W21, T56, Y38, and the heme propionate arms. In WT DHP B, T56 resides in a different conformation, with the O^γ turned away from the pocket, interacting with the E helix. In line with the lack of a water (sixth) ligand in DHP B (F21W), the distal histidine, H55, does not participate in the H-bond network inside the distal pocket, but instead resides in the solvent-open conformation interacting with the heme propionate arms and a sulfate molecule. The heme was observed in a slightly twisted and domed orientation, with the Fe lying 0.06 \AA below the heme pyrrole N plane (vs 0.21 \AA for ferric WT DHP B [18]). Comparing subunit-averaged distances (Table 4) between DHP B (F21W) and WT DHP B, the Fe–H89 N^ϵ distance is 0.10 \AA longer in the mutant (2.28 vs 2.18 \AA) while the H89 N^δ –L83 carbonyl O distance is shorter by 0.14 \AA (2.73 vs 2.87 \AA). However, the Fe–H89 C^α distances are comparable (6.15 vs 6.13 \AA), suggesting that the differences in H89 distances can be ascribed to the side chain itself and not the protein backbone. Additionally, Fe–H55 C^α distances (8.69 vs 8.67 \AA) and Fe– C^α distances for residue 21 (W21: 10.65 \AA vs F21: 10.75 \AA) show very little deviation between mutant and wild-type main chain distances, resulting in similar heme pocket geometries.

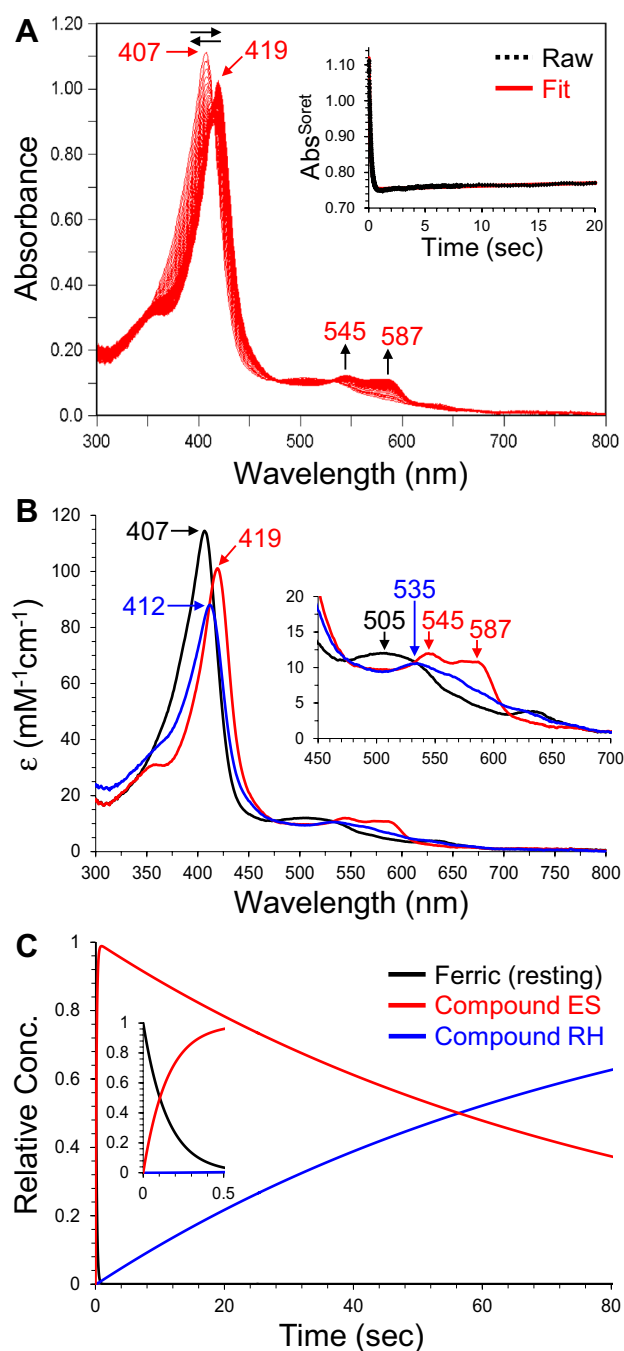


Fig. 4 Kinetic data obtained by optical spectroscopy for the reaction of DHP B (F21W) with H_2O_2 . **a** Stopped-flow UV–visible spectra of the reaction of DHP B (F21W) (10 μM) with a ten-fold excess of H_2O_2 at pH 7 (900 scans over 83 s); inset—the single wavelength (407 nm) dependence on time obtained from the raw spectra and its fit with a superposition of the calculated spectra components; **b** Calculated spectra of the three reaction components derived from the SVD analysis: ferric (black), compound ES (red), and compound RH (blue); **c** time dependences of the relative concentrations for the three components shown in panel B

Discussion

Using the previous study of Dawson and co-workers [24] as inspiration for the present work, the F21W mutation was rationally designed with the intention of blocking the $\text{TCP}_{\text{interior}}$ binding site in an effort to increase the selectivity of DHP as a peroxygenase enzyme at the expense of its peroxidase activity. To that end, the DHP B (F21W) mutant exhibited minimal decreases in peroxygenase activity of 1.2–2.1-fold as measured by substrate conversion, whereas the catalytic efficiency of the peroxidase activity was more than sevenfold decreased. Interestingly, Dawson and co-workers showed that the catalytic efficiency for DHP A (F21W) peroxidase reactivity was reduced 15-fold compared to WT DHP A [24]. Thus, the question arose as to why the effect of the F21W mutation is more muted in DHP B than in DHP A. From a structural standpoint, the differences in primary structure between these two isoenzymes are limited to five amino acid substitutions (note—isoenzyme A is listed first): I/L9, R/K32, Y/N34, N/S81 and S/G91. These amino acid substitutions do not perturb the overall structural fold of DHP when comparing the two isoenzymes [18], yet they result in DHP B exhibiting a greater reactivity than DHP A for both peroxidase and peroxygenase activities [4, 5, 9]. However, why the F21W mutation affects DHP A more than DHP B cannot be addressed by a simple structural comparison (*vide infra*).

To begin to address this question, we performed stopped-flow UV/visible spectroscopic studies to assess whether the formation of the compound ES intermediate in DHP B (F21W) was altered owing to the introduction of a redox-active tryptophan residue near the active site. However, no significant differences in the rates of formation and decay, or in its spectral features, were noted for compound ES, suggesting that the introduction of the F21W mutation does not alter the electronic structure of this reactive intermediate. Similarly, we were concerned if the F21W mutation alters the oxidation pathway of haloindoles (i.e., causes a switch from O atom transfer to electron transfer); however, isotope labeling studies confirmed the peroxygenase mechanism of DHP remains intact in DHP B (F21W). Taken together, we conclude that the F21W mutation does not significantly change the nature of the catalytic intermediates, and thus does not alter the mechanisms that have been established in DHP for peroxidase [2] and peroxygenase [4–6] activities.

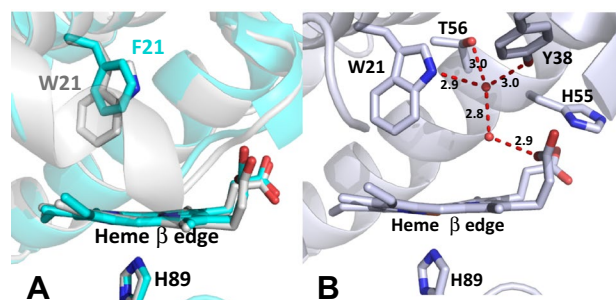
Having ruled out changes to the catalytic intermediates as being responsible for the differences in activity between DHP A (F21W) and DHP B (F21W), we considered structural (and potentially dynamic) effects of the catalytically relevant proximal and distal histidine

Table 2 Comparison of UV–visible spectroscopic data for the ferric, compound ES, and compound RH species in DHP B (F21W) and WT DHP isoenzymes A and B at pH 7

Enzyme	Ferric ^a	Compound ES	Compound RH	References
DHP B (F21W)	407, 505, 535 (sh) 635	419, 545, 587	412, 535, 565	^b
WT DHP A	407, 504, 538, 635	420, 545, 585	411, 530, 564	[8]
WT DHP B	407, 508, 633	419, 545, 585	411, 554, 599	[9]

^a Values reported are in nm^b This work**Table 3** X-ray data collection and refinement statistics for DHP B (F21W) (5VLX)

PDB accession code	5VLX
Data collection	
Wavelength (Å)	1.54
Temperature (K)	100
Space group	P2 ₁ 2 ₁ 2 ₁
Unit-cell parameters (Å)	
a	60.48
b	67.13
c	67.37
Unique reflections	25,631 (1032) ^a
Completeness (%)	97.8 (80.2) ^a
R _{merge} (%) ^b	8.4 (39.5)
I/σ _(I)	25.0 (2.4) ^a
Redundancy	4.5 (3.3) ^a
V _m (Å ³ /Da)	2.21
Refinement	
Resolution (Å)	1.80
R _{work} (%) ^c	16.62 (21.59) ^a
R _{free} (%) ^d	20.44 (29.75) ^a
No. of protein atoms	2317
No. of solvent atoms	215
R.m.s.d from ideal geometry ^e	
Bond lengths (Å)	0.007
Bond angles (°)	0.926
Ramachandran plot (%)	
Most favored region	98.89
Add allowed region	1.11

^a Values in parentheses are for the highest resolution shell^b $R_{\text{merge}} = \frac{\sum_h \sum_i |I_i(h) - \langle I(h) \rangle|}{\sum_h \sum_i I_i(h)} \times 100\%$, where $I_i(h)$ is the i th measurement and $\langle I(h) \rangle$ is the weighted mean of all measurements of $I(h)$ ^c $R_{\text{work}} = \frac{\sum |F_o - F_c|}{\sum F_o} \times 100\%$, where F_o and F_c are the observed and calculated structure factors, respectively^d R_{free} is the R factor for the subset (7.8%) of reflections selected before and not included in the refinement^e Root-mean-square deviation^f Ramachandran plot created via MolProbity**Fig. 5** a DHP B (F21W) (silver) C^α superposition with WT DHP B (cyan; PDB 3IXF [18]), highlighting the F21/W21 residues. Only one conformation for F21 is shown for clarity. b Distal pocket of the DHP B (F21W) mutant, as viewed from the heme β edge. There are two water molecules in the distal pocket, forming a H-bonding network with W21, T56, Y38, and the heme propionate arms. All distances are given in Å**Table 4** Selected distances (Å) for DHP B (F21W) and WT DHP B (PDB accession 3IXF [18])

	DHP B (F21W)		WT DHP B ^a	
	Protomer A	Protomer B	Protomer A	Protomer B
Fe–H89 N ^ε	2.28	2.27	2.18	2.17
H89 N ^δ –L83 O	2.71	2.74	2.92	2.81
Fe–H89 C ^α	6.16	6.14	6.14	6.11
Fe–H55 C ^α	8.61	8.77	8.71	8.63
Fe–F21/W21 C ^α	10.67	10.63	10.76	10.74
Fe–F21/W21 Side chain	5.06 (C ^η)	5.03 (C ^η)	6.50 (C ^ξ)	6.32 (C ^ξ)
	5.47 (C ^{ξ2})	5.49 (C ^{ξ2})	6.74 (C ^{ε1})	6.60 (C ^{ε1})

^a For clarity, only distances for the F21 conformer closest to the heme are given for WT DHP B

residues. Our rationale for such a consideration is that it has been previously shown that tuning of DHP activity may be accomplished by altering (i) the proximal cavity charge relay [11, 38] that includes histidine (H89), whose role is to facilitate dioxygen binding to the ferrous heme or to support the Fe(IV) oxidation state in compounds I, ES and II, and (ii) the conformational flexibility and/

or position of the catalytically important distal histidine (H55) [39–41], which is critical for enzyme activation (i.e., cleavage of compound 0 to the activated ferryl species). In the context of the structure–function relationship ascribed to these two residues, we propose the following five factors that may individually, or in combination, account for the differential effect of the F21W mutation in DHP A and B when compared to the WT isoenzymes: (1) DHP possesses a Leu-His-Fe charge relay (as opposed to the typical peroxidase Asp-His-Fe one) whose function is to stabilize the ferryl intermediates through polarization of the proximal histidine [2, 11]. In DHP B (F21W), the H89 N^δ–83 carbonyl O distance of 2.72 Å is shorter by 0.14 Å than that found in WT DHP B (2.87 Å), and would better support a ferryl intermediate. (2) The distal histidine is unusually flexible in DHP, being normally found in equilibrium between the “open” (5cHS) and “closed” (6cHS, water-bound) states in the WT isoenzymes. It has been hypothesized [1, 25, 26, 42–44] that altering this conformational flexibility may affect substrate/co-substrate binding by gating the accessibility of the active site pocket for entry/exit of substrate/product molecules or co-substrate H₂O₂ [2, 40]. In DHP B (F21W), the distal histidine was only found in the ‘open’ (5cHS) solvent-accessible conformation, stabilized by H-bonding interactions with the heme propionate arms and an exogenous sulfate ion. This ‘open’ conformation of H55 enables the presence of active site waters by excluding the H55 from the distal pocket. (3) Although no water ligand was found to bind the heme-Fe in both protomers (a feature that has commonly been observed in ferric DHP structures [18, 44]), two water molecules were found in the distal pocket. The introduction of a nitrogen-containing indole ring from the tryptophan side chain likely increases the polarity of the distal pocket, creating a more attractive environment for accommodating water molecules in the active site. The presence of these distal waters also involves a H-bonding network that includes the O^γ of the T56 side chain (now unable for stabilization of Helix E), Y38 (site of radical formation in DHP B), a heme propionate arm, and W21. (4) In studies of the T56 mutants of DHP [39], a greater conformational flexibility of the distal histidine was noted. In DHP B (F21W), it was noted that the O^γ of the T56 side chain was positioned into the distal pocket instead of its normal role of stabilization of helix E, which could lead to altered H55 flexibility. (5) Although no crystal structure of DHP A (F21W) is available, calculations showed that the orientation of the W21 side chain was directed away from the heme iron and toward the δ heme edge [24]. In the DHP B (F21W) crystal structure, however, W21 was observed positioned directly toward the heme-Fe, which would likely alter the reactivity in comparison to that of isoenzyme A mutant.

On the whole, the introduction of the F21W mutation causes very little structural perturbation relative to the wild-type structure. As shown by the C^α superposition, the heme retains the same position and orientation, which was unexpected given the increased size of the tryptophan side chain compared to that of phenylalanine. The most notable difference between the F21W mutant and WT structure was observed in the side chain distances for the mutated residue. Remarkably, however, the protein backbone and remaining parts of the structure were virtually identical in spite of the steric differences imposed by the larger indole ring. As expected for the F21W mutation, the tryptophan side chain is in closer proximity to the heme cofactor. Averaging subunits, in WT DHP B the closest atom of the phenyl ring to the heme Fe is C^ε at a distance of 6.41 Å, with C^ε¹ as the next closest atom at 6.67 Å. In the F21W mutant, the C^η atom resides 5.05 Å from the heme Fe with the next closest atom, C^ε² located 5.48 Å from the Fe. Thus, when compared to F21 in WT DHP B, W21 has a contact ~ 1.3 Å closer to the heme Fe. As a consequence, W21 effectively resides in the TCP_{interior} binding site [24] (Fig. 6a), which can be directly related to the attenuation of peroxidase reactivity. However, peroxidase activity is still observed, which may be explained by the presence of a second TCP binding site (TCP_{exterior}). This shows that while the TCP_{interior} binding site has a significant role in TCP oxidation, it is not solely responsible for TCP reactivity, and the TCP_{exterior} binding site may play a functional role as well through long-range electron transfer.

As has been established for DHP, the presence of peroxidase substrates within the heme pocket does not follow the normally observed peroxidase substrate binding motif at the heme γ or δ edge [2]. DHP thus presents an unconventional example of observed internal binding of substrates that undergo oxidation through a mechanism that is generally characterized by substrate binding external of the heme cavity [45]. Internal peroxidase substrate binding is an obvious consequence of the unusually large distal cavity presented in DHP (even though the tertiary structure possesses a

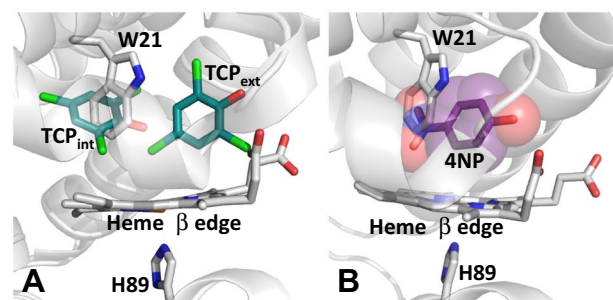


Fig. 6 DHP B (F21W) mutant distal pocket superposition with TCP [TCP_{interior} (PDB 4KMV) and TCP_{exterior} (PDB 4KMW) [24]] and 4-NP (PDB 5CHQ [4]) substrates

traditional globin fold), which is spacious enough to accommodate internal binding of phenolic peroxidase substrates. Thus, the peroxidase mechanism of DHP may in fact exclude the generally observed requirement of external substrate binding, with the two sequential one-electron oxidation steps [15] possibly occurring within the distal cavity.

Peroxygenase reactivity, on the other hand, is characterized by atom transfer, and to facilitate this transfer the substrate binding sites have greater constraints on their possible orientations and distances from the activated ferryl intermediate. W21 only partially overlaps with the 4-NP binding site [4] (Fig. 6b), specifically with the nitro group of 4-NP, but not with the bulk of the 4-NP substrate. The limited steric clash with the nitro group of 4-NP likely still permits it to bind in an orientation that is in close proximity to the activated heme Fe, which in turn would appear to permit oxygen atom transfer as required for the peroxygenase mechanism. Crystallographic substrate binding sites of 5-Br-indole and 7-Br-indole have yet to be obtained, however, computationally [5] derived binding sites are in good agreement with spectroscopic data: (i) 5-Br-indole has been computed to bind in the distal pocket above the heme Fe, which correlates to the substrate's perturbation of the 5cHS/6cHS heme equilibrium to favor the 5cHS species; (ii) the 7-Br-indole computed binding site resides deeper in the distal pocket, and consequently the binding of 7-Br-indole has little or no effect on the 5cHS/6cHS heme equilibrium, indicating this substrate binds in an orientation that does not inhibit water ligation to the heme Fe. In DHP B (F21W), the additional steric bulk of the W21 side chain is in a position to hinder 5-Br-indole binding while not fully blocking the binding site. This was reflected in the dissociation constant for 5-Br-indole in DHP B (F21W) ($K_d = 2960 \pm 940 \mu\text{M}$; Fig. S1) being 20-fold higher than in WT DHP B ($K_d = 150 \pm 10 \mu\text{M}$), which likely results from either weaker binding in the same site as the WT enzyme, or possibly that binding occurs at a different site. In agreement with the computed binding of 7-Br-indole showing that this substrate resides deeper in the distal pocket, the additional steric bulk of W21 appears to have a very small effect on 7-Br-indole reactivity, with a decrease of only 1.2-fold.

Conclusion

The DHP B (F21W) mutant was rationally designed in an effort to decrease peroxidase reactivity through perturbation of the peroxidase substrate binding site, with a minimal (albeit non-zero) consequence on peroxygenase activity. As such, the F21W mutation enables the selective tuning of activity in this multifunctional hemoprotein. The results provide further evidence that confirm the plasticity of the DHP heme distal cavity: namely, the distal cavity of DHP

can accommodate large substrates (i.e., haloindoles) and increases in side chain volume (i.e., Phe \rightarrow Trp) while maintaining a nearly identical backbone structure. The dominant change in the side chains appears restricted to the position of the distal histidine in that it is forced into the solvent-exposed conformation. This change does have functional consequences, although it does not itself constitute an off switch—surprisingly, the activation of bound H_2O_2 is robust and appears to be possible even in a structure where H55 is forced into the external position through the combination of binding a large substrate and a large side chain. Thus, the F21W mutant confirms that H_2O_2 -binding and subsequent enzyme activation may still be possible even when H55 is forced into the external position. Our studies here therefore suggest that it may be possible to further tune DHP activity through simultaneous mutagenesis of multiple active site residues without the requirement that the distal histidine be positioned in the internal conformation to serve as the general acid/base catalyst of the Poulos–Kraut mechanism.

Acknowledgements This project was supported by NSF CAREER Award CHE-1150709 and NSF CHE-1609446. Mass spectra were obtained at the Mass Spectrometry Facility for Biotechnology at North Carolina State University. Partial funding for the facility was obtained from the North Carolina Biotechnology Center and the National Science Foundation.

References

- Lebioda L, LaCount MW, Zhang E, Chen YP, Han K, Whitton MM, Lincoln DE, Woodin SA (1999) *Nature* 401:445
- Franzen S, Ghiladi RA, Lebioda L, Dawson J (2016) *Heme peroxidases*. The Royal Society of Chemistry, Cambridge, pp 218–244
- Chen YP, Woodin SA, Lincoln DE, Lovell CR (1996) *J Biol Chem* 271:4609–4612
- McCombs NL, D'Antonio J, Barrios DA, Carey LM, Ghiladi RA (2016) *Biochemistry* 55:2465–2478
- Barrios DA, D'Antonio J, McCombs NL, Zhao J, Franzen S, Schmidt AC, Sombers LA, Ghiladi RA (2014) *J Am Chem Soc* 136:7914–7925
- McCombs NL, Smirnova T, Ghiladi RA (2017) *Catal Sci Technol* 7:3104–3118
- Osborne RL, Taylor LO, Han KP, Ely B, Dawson JH (2004) *Biochem Biophys Res Commun* 324:1194–1198
- Feducia J, Dumarieh R, Gilvey LB, Smirnova T, Franzen S, Ghiladi RA (2009) *Biochemistry* 48:995–1005
- D'Antonio J, D'Antonio EL, Thompson MK, Bowden EF, Franzen S, Smirnova T, Ghiladi RA (2010) *Biochemistry* 49:6600–6616
- Thompson MK, Franzen S, Ghiladi RA, Reeder BJ, Svislunenko DA (2010) *J Am Chem Soc* 132:17501–17510
- D'Antonio EL, D'Antonio J, de Serrano V, Gracz H, Thompson MK, Ghiladi RA, Bowden EF, Franzen S (2011) *Biochemistry* 50:9664–9680
- D'Antonio J, Ghiladi RA (2011) *Biochemistry* 50:5999–6011
- Dumarieh R, D'Antonio J, Deliz-Liang A, Smirnova T, Svislunenko DA, Ghiladi RA (2013) *J Biol Chem* 288:33470–33482
- Osborne RL, Sumithran S, Coggins MK, Chen YP, Lincoln DE, Dawson JH (2006) *J Inorg Biochem* 100:1100–1108

15. Osborne RL, Coggins MK, Raner GM, Walla M, Dawson JH (2009) *Biochemistry* 48:4231–4238
16. Davydov R, Osborne RL, Shanmugam M, Du J, Dawson JH, Hoffman BM (2010) *J Am Chem Soc* 132:14995–15004
17. Du J, Sono M, Dawson JH (2010) *Biochemistry* 49:6064–6069
18. de Serrano V, D'Antonio J, Franzen S, Ghiladi RA (2010) *Acta Cryst D66*:529–538
19. Poulos TL, Kraut J (1980) *J Biol Chem* 255:8199–8205
20. Dunford HB (2016) *Heme peroxidases*. The Royal Society of Chemistry, Cambridge, pp 99–112
21. Ortiz de Montellano PR (ed) (2015) *Cytochrome p450: structure, mechanism, and biochemistry*. Springer International Publishing, Switzerland
22. Franzen S, Thompson MK, Ghiladi RA (2012) *Biochim Biophys Acta* 1824:578–588
23. McCombs NL, Moreno-Chicano T, Carey LM, Franzen S, Hough MA, Ghiladi RA (2017) *Biochemistry* 56:2294–2303
24. Wang C, Lovelace LL, Sun S, Dawson JH, Lebioda L (2013) *Biochemistry* 52:6203–6210
25. LaCount MW, Zhang E, Chen YP, Han K, Whitton MM, Lincoln DE, Woodin SA, Lebioda L (2000) *J Biol Chem* 275:18712–18716
26. Thompson MK, Davis MF, de Serrano V, Nicoletti FP, Howes BD, Smulevich G, Franzen S (2010) *Biophys J* 99:1586–1595
27. Zhao J, de Serrano V, Le P, Franzen S (2013) *Biochemistry* 52:2427–2439
28. Beers RF Jr, Sizer IW (1952) *J Biol Chem* 195:133–140
29. Otwinowski Z, Minor W (1997) In: Carter CW Jr, Sweet RM (eds) *Methods in enzymology*. Academic, New York, pp 307–326
30. McCoy AJ, Grosse-Kunstleve RW, Adams PD, Winn MD, Storoni LC, Read RJ (2007) *J Appl Crystallogr* 40:658–674
31. Adams PD, Afonine PV, Bunkoczi G, Chen VB, Davis IW, Echols N, Headd JJ, Hung LW, Kapral GJ, Grosse-Kunstleve RW, McCoy AJ, Moriarty NW, Oeffner R, Read RJ, Richardson DC, Richardson JS, Terwilliger TC, Zwart PH (2010) *Acta Cryst D66*:213–221
32. Emsley P, Lohkamp B, Scott WG, Cowtan K (2010) *Acta Cryst D66*:486–501
33. Afonine PV, Grosse-Kunstleve RW, Echols N, Headd JJ, Moriarty NW, Mustyakimov M, Terwilliger TC, Urzhumtsev A, Zwart PH, Adams PD (2012) *Acta Cryst D68*:352–367
34. Chenprakhon P, Sucharitakul J, Panijpan B, Chaiyen P (2010) *J Chem Educ* 87:829–831
35. Carugo O, Pongor S (2001) *Protein Sci* 10:1470–1473
36. Cohen FE, Sternberg MJ (1980) *J Mol Biol* 138:321–333
37. Chothia C, Lesk AM (1986) *EMBO J* 5:823–826
38. Sun S, Sono M, Wang C, Du J, Lebioda L, Dawson JH (2014) *Arch Biochem Biophys* 545:108–115
39. Jiang S, Wright I, Swartz P, Franzen S (2013) *Biochimica et Biophysica Acta (BBA) Proteins and Proteomics* 1834:2020–2029
40. Zhao J, de Serrano V, Dumariéh R, Thompson M, Ghiladi RA, Franzen S (2012) *J Phys Chem B* 116:12065–12077
41. Carey LM, Gavenko R, Svistunenko DA, Ghiladi RA (2017) *Biochimica et Biophysica Acta (BBA) Proteins and Proteomics* (in press)
42. de Serrano VS, Davis MF, Gaff JF, Zhang Q, Chen Z, D'Antonio EL, Bowden EF, Rose R, Franzen S (2010) *Acta Cryst D66*:770–782
43. Chen Z, de Serrano V, Betts L, Franzen S (2009) *Acta Cryst D65*:34–40
44. de Serrano V, Chen Z, Davis MF, Franzen S (2007) *Acta Cryst D63*:1094–1101
45. Kwon H, Moody PCE, Raven EL (2016) *Heme peroxidases*. The Royal Society of Chemistry, Cambridge, pp 47–60

Affiliations

Leiah M. Carey¹ · Kyung Beom Kim^{1,2} · Nikolette L. McCombs¹ · Paul Swartz³ · Cheal Kim² · Reza A. Ghiladi¹ 

✉ Reza A. Ghiladi
Reza_Ghiladi@ncsu.edu

¹ Department of Chemistry, North Carolina State University, Raleigh, NC 27695-8204, USA

² Department of Fine Chemistry, Seoul National University of Science and Technology, Seoul 139-743, Korea

³ Department of Structural and Molecular Biochemistry, North Carolina State University, Raleigh, NC 27695-7622, USA